URSI-B EMTS 2025, Bologna, 23–27 June

6-Port Topological Valley Junction for Signal Routing

Christian Johnson-Richards (1), Ross Glyn MacDonald (1), Alex Yakovlev (2), and Victor Pacheco-Peña (1)
(1) School of Mathematics, Statistics and Physics, Newcastle University, Newcastle Upon Tyne, NE1 7RU, United Kingdom.
(2) School of Engineering, Newcastle University, Newcastle Upon Tyne, NE1 7RU, United Kingdom

Abstract

Topological waveguides are a nascent and promising technology to provide high transmission without reflection from defects including sharp bends. In this work, the routing of information using multiple incident signals within a 6-port topological valley junction is presented. To achieve this, the scattering matrix that describes the behavior of the 6-port junction is extracted. This is then implemented to calculate incident signals that produce desired outputs. Two cases are considered as illustrative examples: Case A, where the signals are routed to ports 1 and 3, and Case B, where the signals are routed to ports 1 and 5. The results to be shown in this work will demonstrate the potential of multiple interconnected topological waveguides and their analytical model. The latter could allow the design of larger networks that may perform linear analogue processes without the need of using computationally intensive trial and error methods.

1. Introduction

The control of electromagnetic wave propagation has been one of the fundamental aspect of studies in fields including photonics and metamaterials [1-8]. In photonics, Valley photonic crystals (VPCs) are an example of carefully designed structures that enable unique control of light. They consist of photonic topological insulators that are designed to break inversion symmetry [9]. In such devices, a single forward and reverse edge state is supported at the interface between two VPCs with opposite valley-Chern number [10]. VPC-VPC waveguides have demonstrated (alongside other photonic topological insulators) unique properties such as reduced scattering through sharp bends and from large defects in the geometry of the VPCs [11]. Applications include the emulation of linear logic gates [12], routing [13], quantum circuits [14] and the conversion between valley and spin edge states [15].

In this work we build on the works developed by our group in the context of perfect splitting for linear computing [15-21] to investigate a 6-port VPC-VPC waveguide junction that supports equal power splitting at telecoms wavelengths (≈ 1550 nm). Here, perfect splitting refers to the equal splitting of signals at a junction by magnitude including a signal reflected towards the incident port and a phase difference between the reflected and transmitted signals of π [23]. On the other hand, we will refer to equal power splitting as the splitting of signals at a junction with no reflection [23]. To do this, a scattering matrix that represents the splitting of signals at this junction is first extracted [24,25]. This enables the design of linear analogue routing operations. For instance, in this work the scattering matrix is used to inverse calculate the required incident signals for the following two examples: Case A, where the signals are routed towards ports 1 and 3, and case B, where the signals are routed towards ports 1 and 5 (where P_N represents port N, see Figure 1b).

2. Results and Discussion

In our work, the VPCs are modelled in two-dimensions (2D) and are designed with a hexagonal unit cell displayed in Figure 1a, with a lattice constant, $a = 340$ nm and lattice vectors of $\boldsymbol{a_1} = a\hat{\boldsymbol{x}}$ and $\boldsymbol{a_2} = (a/2)\hat{\boldsymbol{x}} + (a\sqrt{3}/2)\,\hat{\boldsymbol{y}}$. Silicon is used as the background material and two air holes are placed in the unit cell, centered at positions $\boldsymbol{p_1} = 1/3(\boldsymbol{a_1} + \boldsymbol{a_2})$ and $\boldsymbol{p_2} = 2/3(\boldsymbol{a_1} + \boldsymbol{a_2})$. Inversion symmetry of the unit cell is then broken by choosing the diameter of the two holes to be unequal. This enables the existence of a bandgap required for VPCs [9]. In doing so, however, two possible VPC orientations are created: an $\uparrow$ (up)-orientated VPC and a $\downarrow$ (down)-orientated VPC (where the arrows point vertically from large holes to small holes, as shown in Figure 1). The diameter of the holes is chosen such that the larger hole has a diameter $d_1 = 0.24a$ and the smaller hole a diameter of $d_2 = 0.12a$. The lattice constant and hole sizes are chosen to place the bulk VPC bandgap centered at wavelength of 1550 nm.

The 6-port junction is then designed by rotating a VPC-VPC waveguide clockwise around the center of the junction (see Figure 1b where the VPC segments have been labelled with corresponding $\uparrow$ and $\downarrow$ arrows). It is at the 6 interfaces between $\uparrow$ and $\downarrow$ VPC segments that the VPC-VPC edge states are located (interfaces are indicated with a thick black line in Figure 1b). Each VPC-VPC interface acts as a port of the 6-port junction and are labelled accordingly in Figure 1b. As it will be explained in detail at the conference a frequency dependent scattering matrix of the structure, $\boldsymbol{S}$, is extracted within the spectral range of $185 \leq f \leq 201$ THz. Interestingly, it will be shown how, indeed, there exists a frequency where the signal is equally divided between three output ports. As an example, a signal applied at P_2 will be split between $P_{1,3,5}$ (as depicted in Figure 1b by the blue and green signals). As it will be shown in the conference, the equal power splitting frequency is $f_s \approx 192.08$ THz.

For this study two cases of wave routing are described: case A includes designed inputs that produce equal magnitude outputs at $P_{1,3}$ and in case B the inputs are modified to produce outputs at $P_{1,5}$. The inputs/outputs can be calculated from the retrieved scattering matrix when considering input vectors of length 6 in the form, $\boldsymbol{X} = [x_1, \dots, x_6]$, where x_N represents an input signal at port N in phasor form. Similarly, an output vector is defined as $\boldsymbol{Y} = [y_1, \dots, y_6]$, where y_N represents an output signal at port N. The resultant output vectors can be calculated following, $\boldsymbol{Y} = \boldsymbol{SX}$ [23], equally the required inputs can be calculated using the inverse of this equation.

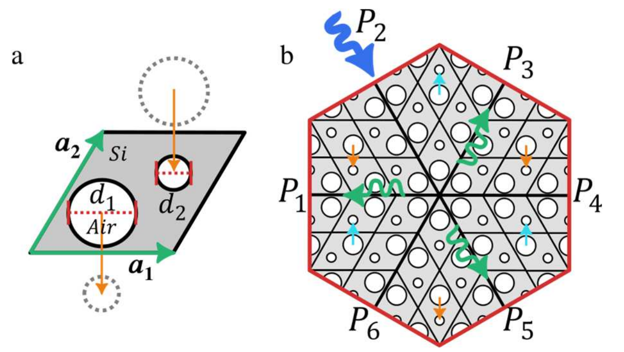

Figure 1. (a) Schematic respresentation of a hexagonal VPC unit cell with side length a and air hole diameters d_1 and d_2. The holes of the adjacent unit cells (above and below) are shown as dashed grey circles. The VPC orientation are marked with orange arrows. (b) Schematic of the 6-port junction designed with two VPCs with orientations marked with ↓/↑-arrows (orange) and light-blue arrows respectively. In this example a single input signal is incident at P_2 (blue) resulting in scattering at the junction that produces output signals towards $P_{1,3,5}$ (green).

To calculate the required input vector for each case it is first considered that equal magnitude inputs were applied at $P_{2,6}$, with the input vector, $\boldsymbol{X} = [0\ ,1e^{i\phi_2}, 0,0,0,1e^{i\phi_6}]$. Then while fixing $\phi_2 = 0$ and utilizing $\boldsymbol{S}$ interpolated to the frequency of equal power splitting, $f = f_s$, it is possible to derive the required values of ϕ_6 that satisfy each case. This results in values of $\phi_6 = \phi_A \approx -1.05$ and $\phi_6 = \phi_B \approx 1.05$ radians for case A and B respectively. For completeness the resulting output vector for case A is $\boldsymbol{Y_A} \approx [1e^{i(-2.62)}, 0, 1e^{i(-1.57)}, 0,0,0]$ and for case B $\boldsymbol{Y_B} \approx [1e^{i(-1.57)}, 0,0,0, 1e^{i(-0.52)}, 0]$.

Given the input vector $\boldsymbol{X}$ and the two input phase conditions ϕ_A and ϕ_B, a 2D numerical study of the junction is carried out. Each VPC segment is extended to cover a square simulation area with a side length of $63a$ and an absorbing region of length $43a$ (not shown in Figure 2) on each side. The two input signals are applied at $P_{2,6}$ at a distance of $30.5a$ from the center of the simulation using point sources orientated so their electric field component is parallel with the VPC-VPC interface.

With this configuration, the numerical results showing the out-of-plane magnetic field for case A are shown in Figure 2a, where it can be seen how the signals applied at ports $P_{2,6}$ are routed towards $P_{1,3}$ with negligible transmission to any other ports or any reflection to the input ports. The results for case B are presented in Figure 2b where it is observed that the inputs at $P_{2,6}$ are routed, instead, towards $P_{1,5}$, similarly with negligible transmission or reflection to any other ports, as expected. During the conference further examples will be shown such as the case where output signals only exist at $P_{3,5}$, a wave director that routes three input signals incident at $P_{1,3,5}$ towards one output signal at P_4 and a study into the performance of the junction with added defects at the center.

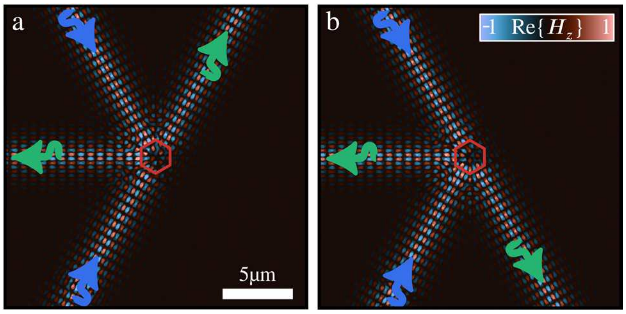

Figure 2. Re$\{H_z\}$ field distributions at a frequency $f = f_s$ for the two cases of wave directing. Both cases consider excitation using an input vector $\boldsymbol{X}$. a) Case A, $\phi_6 = \phi_A \approx -1.05$ and b) case B, $\phi_6 = \phi_B \approx 1.05$. Input/ouput signals are overlayed ontop of the field distributions for both cases in dark blue and green respectively. The red hexagon represents the same area as the red hexagon in Figure 1b.

3. Conclusion

Our recent efforts to exploit the linear routing capabilities of a 6-port VPC junction have been presented. This has been done by extracting the scattering matrix and using inverse calculations to retrieve the required inputs for two routing cases. The device presented along with the scattering matrix could allow for the design of larger networks of junctions that may perform more complex linear computing processes. During the conference, details of the 6-port junction with different input configurations and the effect of removing holes at the center of the junction on the topological protection will be presented.

4. Acknowledgements

This work was supported by the Leverhulme Trust under the Leverhulme Trust Research Project Grant scheme (No. RPG-2020-316 and RPG-2023-024). For the purpose of Open Access, the authors have applied a CC BY public copyright license to any Author Accepted Manuscript (AAM) version arising from this submission.

5. References

[1] R. E. Jacobsen, A. V. Lavrinenko, and S. Arslanagić, 'Reconfigurable dielectric resonators with imbedded impedance surfaces—From enhanced and directional to suppressed scattering', *Appl. Phys. Lett.*, vol. 122, no. 8, p. 081701, Feb. 2023, doi: 10.1063/5.0139695.

[2] C. Tripon-Canseliet *et al.*, 'Optically Controlled Gain Modulation for Microwave Metasurface Antennas', *Sensors*, vol. 24, no. 6, p. 1911, Mar. 2024, doi: 10.3390/s24061911.

[3] V. Pacheco-Peña and N. Engheta, 'Merging Effective Medium Concepts of Spatial and Temporal Media: Opening new avenues for manipulating wave-matter interaction in 4D', *IEEE Antennas Propag. Mag.*, vol. 65, no. 4, pp. 39–49, Aug. 2023, doi: 10.1109/MAP.2023.3254480.

[4] V. Nikkhah *et al.*, 'Inverse-designed low-index-contrast structures on a silicon photonics platform for vector–matrix multiplication', *Nat. Photonics*, vol. 18, no. 5, pp. 501–508, May 2024, doi: 10.1038/s41566-024-01394-2.

[5] H. Moussa, G. Xu, S. Yin, E. Galiffi, Y. Ra'di, and A. Alù, 'Observation of temporal reflection and broadband frequency translation at photonic time interfaces', *Nat. Phys.*, vol. 19, no. 6, pp. 863–868, Jun. 2023, doi: 10.1038/s41567-023-01975-y.

[6] I. Liberal, A. Ganfornina-Andrades, and J. E. Vázquez-Lozano, 'Spatiotemporal Symmetries and Energy-Momentum Conservation in Uniform Spacetime Metamaterials', *ACS Photonics*, vol. 11, no. 12, pp. 5273–5280, Dec. 2024, doi: 10.1021/acsphotonics.4c01496.

[7] V. Pacheco-Peña, Y. Kiasat, D. M. Solís, B. Edwards, and N. Engheta, 'Holding and amplifying electromagnetic waves with temporal non-Foster metastructures', Apr. 07, 2023, *arXiv*: arXiv:2304.03861. doi: 10.48550/arXiv.2304.03861.

[8] L. Stefanini *et al.*, 'Time-Varying Metasurfaces for Efficient Surface-Wave Coupling to Radiation and Frequency Conversion', *Laser Photonics Rev.*, vol. 18, no. 12, p. 2400315, 2024, doi: 10.1002/lpor.202400315.

[9] D. Bisharat, R. Davis, Y. Zhou, P. Bandaru, and D. Sievenpiper, 'Photonic Topological Insulators: A Beginner's Introduction [Electromagnetic Perspectives]', *IEEE Antennas Propag. Mag.*, vol. 63, no. 3, pp. 112–124, Jun. 2021, doi: 10.1109/MAP.2021.3069276.

[10] Y. Kawaguchi *et al.*, 'Pseudo-spin switches and Aharonov-Bohm effect for topological boundary modes', *Sci. Adv.*, vol. 10, no. 15, p. eadn6095, Apr. 2024, doi: 10.1126/sciadv.adn6095.

[11] T. Ozawa *et al.*, 'Topological photonics', *Rev. Mod. Phys.*, vol. 91, no. 1, p. 015006, Mar. 2019, doi: 10.1103/RevModPhys.91.015006.

[12] M.-H. Chao, B. Cheng, Q.-S. Liu, W.-J. Zhang, Y. Xu, and G.-F. Song, 'Novel optical XOR/OR logic gates based on topologically protected valley photonic crystals edges', *J. Opt.*, vol. 23, no. 11, p. 115002, Nov. 2021, doi: 10.1088/2040-8986/ac11ac.

[13] J. Ma, X. Xi, and X. Sun, 'Topological Photonic Integrated Circuits Based on Valley Kink States', *Laser Photonics Rev.*, vol. 13, no. 12, p. 1900087, Dec. 2019, doi: 10.1002/lpor.201900087.

[14] Y. Chen *et al.*, 'Topologically Protected Valley-Dependent Quantum Photonic Circuits', *Phys. Rev. Lett.*, vol. 126, no. 23, p. 230503, Jun. 2021, doi: 10.1103/PhysRevLett.126.230503.

[15] J. Ma, X. Xi, Y. Li, and X. Sun, 'Nanomechanical topological insulators with an auxiliary orbital degree of freedom', *Nat. Nanotechnol.*, vol. 16, no. 5, pp. 576–583, May 2021, doi: 10.1038/s41565-021-00868-6.

[16] E. Feigenbaum and M. Orenstein, 'Perfect 4-way splitting in nano plasmonic X-junctions', *Opt Express*, vol. 15, no. 26, pp. 17948–17953, Dec. 2007, doi: 10.1364/OE.15.017948.

[17] A. Yakovlev and V. Pacheco-Peña, 'Enabling High-Speed Computing with Electromagnetic Pulse Switching', *Adv. Mater. Technol.*, vol. 5, no. 12, p. 2000796, 2020, doi: https://doi.org/10.1002/admt.202000796.

[18] V. Pacheco-Peña and A. Yakovlev, 'Computing with Square Electromagnetic Pulses', 2021, pp. 465–492. doi: 10.1142/9789811235740_0016.

[19] R. G. MacDonald, A. Yakovlev, and V. Pacheco-Peña, 'Amplitude-Controlled Electromagnetic Pulse Switching Using Waveguide Junctions for High-Speed Computing Processes', *Adv. Intell. Syst.*, vol. 4, no. 12, p. 2200137, Dec. 2022, doi: 10.1002/aisy.202200137.

[20] A. Ventisei, A. Yakovlev, and V. Pacheco-Peña, 'Exploiting Petri Nets for Graphical Modelling of Electromagnetic Pulse Switching Operations', *Adv. Theory Simul.*, vol. 5, no. 3, p. 2100429, 2022, doi: 10.1002/adts.202100429.

[21] W. Rogers, C. Johnson-Richards, A. Yakovlev, and V. Pacheco-Peña, 'Perfect splitting in rectangular-waveguide junctions for analog computing', *Phys. Rev. Appl.*, vol. 21, no. 5, p. 054054, May 2024, doi: 10.1103/PhysRevApplied.21.054054.

[22] R. G. MacDonald, A. Yakovlev, and V. Pacheco-Peña, 'Solving partial differential equations with waveguide-based metatronic networks', *Adv. Photonics Nexus*, vol. 3, no. 05, Oct. 2024, doi: 10.1117/1.APN.3.5.056007.

[23] D. M. Pozar, *Microwave engineering*. Hoboken, N.J.: Wiley, 2012.

[24] G. Lévêque *et al.* 'Scattering-matrix approach for a quantitative evaluation of the topological protection in valley photonic crystals', *Phys. Rev. A*, vol. 108, no. 4, p. 043505, Oct. 2023, doi: 10.1103/PhysRevA.108.043505.

[25] C. Johnson-Richards, A. Yakovlev, and V. Pacheco-Peña, 'Topological Valley Photonic Waveguides: Scattering matrix evaluation for linear computing', Dec. 03, 2024, *arXiv*: arXiv:2412.02388. doi: 10.48550/arXiv.2412.02388.